Medical Physics
The International Journal of Medical Physics Research and Practice

Automated registration of multispectral MR vessel wall images of the carotid artery

R. van 't Klooster, M. Staring, S. Klein, R. M. Kwee, M. E. Kooi, J. H. C. Reiber, B. P. F. Lelieveldt, and R. J. van der Geest

Citation: Medical Physics **40**, 121904 (2013); doi: 10.1118/1.4829503
View online: http://dx.doi.org/10.1118/1.4829503
View Table of Contents: http://scitation.aip.org/content/aapm/journal/medphys/40/12?ver=pdfcov
Published by the American Association of Physicists in Medicine

Automated registration of multispectral MR vessel wall images of the carotid artery

R. van 't Klooster and M. Staring
Department of Radiology, Division of Image Processing, Leiden University Medical Center, 2300 RC Leiden, The Netherlands

S. Klein
Department of Radiology and Department of Medical Informatics, Biomedical Imaging Group Rotterdam, Erasmus MC, Rotterdam 3015 GE, The Netherlands

R. M. Kwee and M. E. Kooi
Department of Radiology, Cardiovascular Research Institute Maastricht, Maastricht University Medical Center, Maastricht 6202 AZ, The Netherlands

J. H. C. Reiber, B. P. F. Lelieveldt, and R. J. van der Geest[a)]
Department of Radiology, Division of Image Processing, Leiden University Medical Center, 2300 RC Leiden, The Netherlands

(Received 24 December 2012; revised 21 October 2013; accepted for publication 21 October 2013; published 11 November 2013)

Purpose: Atherosclerosis is the primary cause of heart disease and stroke. The detailed assessment of atherosclerosis of the carotid artery requires high resolution imaging of the vessel wall using multiple MR sequences with different contrast weightings. These images allow manual or automated classification of plaque components inside the vessel wall. Automated classification requires all sequences to be in alignment, which is hampered by patient motion. In clinical practice, correction of this motion is performed manually. Previous studies applied automated image registration to correct for motion using only nondeformable transformation models and did not perform a detailed quantitative validation. The purpose of this study is to develop an automated accurate 3D registration method, and to extensively validate this method on a large set of patient data. In addition, the authors quantified patient motion during scanning to investigate the need for correction.
Methods: MR imaging studies (1.5T, dedicated carotid surface coil, Philips) from 55 TIA/stroke patients with ipsilateral <70% carotid artery stenosis were randomly selected from a larger cohort. Five MR pulse sequences were acquired around the carotid bifurcation, each containing nine transverse slices: T1-weighted turbo field echo, time of flight, T2-weighted turbo spin-echo, and pre- and post-contrast T1-weighted turbo spin-echo images (T1W TSE). The images were manually segmented by delineating the lumen contour in each vessel wall sequence and were manually aligned by applying throughplane and inplane translations to the images. To find the optimal automatic image registration method, different masks, choice of the fixed image, different types of the mutual information image similarity metric, and transformation models including 3D deformable transformation models, were evaluated. Evaluation of the automatic registration results was performed by comparing the lumen segmentations of the fixed image and moving image after registration.
Results: The average required manual translation per image slice was 1.33 mm. Translations were larger as the patient was longer inside the scanner. Manual alignment took 187.5 s per patient resulting in a mean surface distance of 0.271 ± 0.127 mm. After minimal user interaction to generate the mask in the fixed image, the remaining sequences are automatically registered with a computation time of 52.0 s per patient. The optimal registration strategy used a circular mask with a diameter of 10 mm, a 3D B-spline transformation model with a control point spacing of 15 mm, mutual information as image similarity metric, and the precontrast T1W TSE as fixed image. A mean surface distance of 0.288 ± 0.128 mm was obtained with these settings, which is very close to the accuracy of the manual alignment procedure. The exact registration parameters and software were made publicly available.
Conclusions: An automated registration method was developed and optimized, only needing two mouse clicks to mark the start and end point of the artery. Validation on a large group of patients showed that automated image registration has similar accuracy as the manual alignment procedure, substantially reducing the amount of user interactions needed, and is multiple times faster. In conclusion, the authors believe that the proposed automated method can replace the current manual procedure, thereby reducing the time to analyze the images. [http://dx.doi.org/10.1118/1.4829503]

Key words: atherosclerosis, carotid artery, vessel wall images, multispectral MRI, image registration

1. INTRODUCTION

Atherosclerosis is the primary cause of heart disease and stroke. These cardiovascular diseases are the leading cause of death in the Western world.[1] Atherosclerosis is a progressive disease which, at an early stage, is characterized by the accumulation of lipids and inflammatory cells in the vessel wall of large arteries, and, at a later stage, by the formation of plaque lesions inside the vessel wall.[2] Identification of vulnerable plaques, lesions with a high risk to rupture which in turn can lead to a cardiovascular event such as stroke, is of high clinical relevance.

Magnetic Resonance Imaging (MRI) of the carotid artery vessel wall is often used to assess atherosclerosis and is one of the most promising imaging modalities for visualizing plaque in the carotid artery. It is noninvasive, does not involve ionizing radiation, and is highly reproducible.[3] Detailed assessment of atherosclerosis in the carotid artery requires high resolution imaging of the vessel wall using multiple MR sequences with different contrast weightings.[4] A MRI examination of the carotid artery usually starts with the acquisition of a time of flight (TOF) magnetic resonance angiography sequence which provides a global overview of the vascular structure. Subsequently, several additional 2D acquisitions can be planned and acquired to obtain information about the vessel wall morphology and plaque composition. These vessel wall images are usually scanned perpendicular to the carotid artery and typically have a high resolution inplane (0.4 mm) and a significantly lower throughplane resolution (3 mm). Manual or automated analysis of the vessel wall images allows identification and quantification of the plaque components inside the vessel wall. Based on this information, the clinically relevant vulnerable plaques can be distinguished from stable plaques.

The duration of a multisequence MRI protocol is between 30 and 60 min. Due to patient movement significant misalignment may occur between the sequences. The effect of patient motion is especially noticeable inplane; a movement of 1 mm by the patient can result in a shift of multiple pixels in the subsequent MR sequence. The effect of movement in the throughplane direction is less obvious due to the lower resolution, but is still present. These translations between different sequences due to patient movement decrease the accuracy of plaque quantification and increase the time needed by a human expert to analyze the images because comparing similar locations between the images is less straightforward due to the inconsistency in the spatial relation between the sequences. Therefore, patient movement should be corrected for.

The current way in clinical research to correct patient movement is manual alignment of the vessel wall images by an expert. First, in one sequence the lumen and outer wall contours are delineated, followed by manual intrascan image alignment by applying a combination of throughplane translation of the complete image stack and inplane translation for individual image slices. The expert takes into account the appearance of the images and uses the lumen and outer wall contours as a reference. Once all images are aligned, regions of plaque can be identified and characterized by evaluating the relative signal intensities in the available imaging sequences. Various schemes for plaque classification have been reported for different imaging protocols, which can be used to identify regions of calcification, lipid core, intraplaque hemorrhage, ulceration, and fibrous tissue.[5–7] In case the segmentation of the plaque components is performed by an automated method,[8–10] accurate alignment of the images is essential since most of these methods classify pixels in the vessel wall using the signal intensities from the different MR sequences, thereby assuming pixelwise correspondence between the images.

Since manual alignment is a user dependent and a time-consuming procedure, automatic image registration has been applied in a number of studies. An overview of these studies is given in Table I. In previous work, registration was mainly performed in 2D,[8,10–12] ignoring any patient movement in the throughplane direction. In all studies, a region of interest around the carotid artery was used and image similarity metrics based on correlation, mutual information (MI), or gradients in the image were used. Transformation models were limited to translation and rotation. Fei *et al.*[13] performed image registration in 3D allowing for translation and rotation in all three directions, and Tang *et al.*[14] used a 3D affine transformation. It is however to be expected that patient motion also results in nonrigid deformation of the carotid vessel wall.[15,16] Another limitation of the above studies is that the registration results were either assessed visually or no validation was performed. Quantitative validation was performed in only one study on five healthy volunteers.[12] To overcome the limitations of these studies, 3D nonrigid image registration methods should be investigated, optimized, and quantitatively validated on a large set of patient data.

Therefore, the purpose of this study was to investigate patient movement during scanning, to develop an accurate automated 3D registration method, and to perform a quantitative validation. The contribution of this study is threefold: (1) the manual alignments of a large number of studies were analyzed to quantify the average patient movement in MR vessel wall studies, thereby motivating the need for correction; (2) the development of an optimal 3D registration method; and (3) to perform a quantitative validation of the registration results using an independent reference standard on a large population.

2. MATERIALS AND METHODS

2.A. Image data

Images from 55 TIA or stroke patients with ipsilateral <70% carotid artery stenosis were randomly selected from a larger cohort.[17] MR images of the stenosed artery were obtained on a 1.5T scanner using a dedicated carotid surface coil (both Philips Healthcare, Best, The Netherlands). Five MR pulse sequences were acquired around the carotid bifurcation, each containing nine transverse slices: 3D T1-weighted turbo field echo (T1W TFE), 3D TOF, 2D T2-weighted turbo spin-echo (T2W TSE), and pre- and postcontrast 2D T1-weighted turbo spin-echo images (T1W TSE), with precise acquisition parameters as described by Kwee *et al.*[18] For all sequences,

TABLE I. Literature overview (ROI = region of interest, MI = mutual information).

Study	Dataset description	Image similarity metric	ROI usage	Transformation model	Validation method
Adame *et al.* (Ref. 11)	19 patients, two MR sequences	Correlation coefficient	Yes	2D translation	None
Biasiolli *et al.* (Ref. 12)	Five volunteers + 20 patients, three MR sequences	Correlation ratio MI Gradient MI	Yes	2D translation + rotation	Five volunteers: quantitative validation. 20 patients: visual validation.
Hofman *et al.* (Ref. 8)	25 patients, five MR sequences	Normalized MI	Yes	2D translation + rotation	None
Liu *et al.* (Ref. 10)	26 patients, five MR sequences	Active edge map	Yes	2D translation	87% correct, no further details given.
Fei *et al.* (Ref. 13)	Two volunteers + one patient, three MR sequences	Normalized MI	Unknown	3D translation + rotation	Visual validation
Tang *et al.* (Ref. 14)	48 patients, two MR sequences	MI	Yes	First 3D rigid, then 3D affine	Visual validation

the field of view was 100 × 80 mm, with a matrix size of 256 × 205 (inplane resolution, 0.39 × 0.39 mm), except for the T1W TFE sequence (field of view, 100 × 80 mm; matrix size, 256 × 163; inplane resolution, 0.39 × 0.49 mm). The slice thickness of the T1W TFE and TOF sequences was 3.0 mm with no slice gap. The slice thickness of the T1W TSE and T2W TSE sequences was 2.5 mm with a slice gap of 0.5 mm. All images were reconstructed to a pixel size of 0.20 × 0.20 mm^2 inplane. This study was approved by the institutional medical ethics committee and all patients gave written informed consent.

2.B. Gold standard

An expert observer with four years of experience in vessel wall analysis traced the lumen boundary of the common or the internal carotid artery in each image slice of each MR sequence in all 55 studies. During delineation, all sequences were shown to the expert, so all image information was available to obtain accurate contours. The set of lumen contours form a manual segmentation and are further referred to as the *gold standard* in the remainder of the paper.

2.C. Manual alignment

A second expert with two years of experience in MRI plaque analysis performed manual alignment and manual segmentation in all 55 studies. Manual alignment was performed by aligning the images from the different sequences to the precontrast T1W TSE image. This sequence is often used to delineate the vessel wall contours and provides a good visualization of the carotid vessel wall and most plaque components. First, the expert delineated the lumen and outer contours of the common or the internal carotid artery in the precontrast T1W TSE sequence, which were then overlaid on the other sequences. Next, the images of the remaining sequences were inspected and a throughplane translation was applied to the complete image stack if needed. Finally, each image slice was aligned to the lumen and outer contours by applying an inplane translation. The set of throughplane and inplane translations defines the manual alignment. The contours which served as an aid for the alignment were not used in the remainder of this paper. All manual alignments and segmentations were performed using a dedicated software package (VesselMASS; Leiden University Medical Center, Leiden, The Netherlands).[19] An example of the image data including manual alignment and lumen contour is shown in Fig. 1.

2.D. Automatic image registration

The goal of automatic image registration is to determine a spatial transformation that relates positions in one image to corresponding positions in another image. After successful registration, information from the different images can be compared, combined, or analyzed.[20] Registration is the process of finding a coordinate transformation $T(x)$ that makes the moving image $I_M(T(x))$ spatially aligned to the fixed image $I_F(x)$. The degrees of freedom of $T(x)$ determine the types of deformation that can be recovered and these deformations are defined by the choice of the transformation model.[21] The registration problem can be formulated as an optimization problem in which a cost function C, which is negatively related to an image similarity metric S, is minimized with respect to T_μ, where T_μ is a parameterization of transformation T and subscript μ represents a vector that contains the values of the transformation parameters

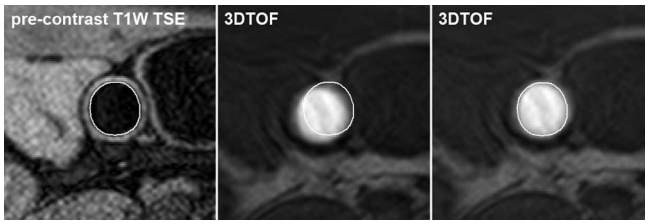

FIG. 1. T1W TSE image (left) with delineated lumen contour (white), TOF image with the T1W TSE lumen contour overlaid showing misalignment (middle), TOF image after manual alignment (right).

$$\hat{\mu} = \arg\min_{\mu} C(T_\mu; I_F, I_M), \tag{1}$$

$$C(T; I_F, I_M) = -S(T; I_F, I_M). \tag{2}$$

This minimization problem is commonly solved by employing an iterative optimization strategy.[22]

There are several choices possible for the transformation model. Performing a 2D translation per image slice is similar to the process of manual alignment by the expert. It provides a 2D translation vector for each image slice. Examples of other transformation models are, in order of increasing flexibility, the rigid, the affine, and the nonrigid B-spline transformation. The rigid transformation treats the image as a rigid body which can translate and rotate. The affine transformation extends the rigid transformation by adding scaling and shearing to the model. The nonrigid transformation is modeled as a weighted sum of B-spline basis functions placed on a uniform control point grid. By moving the control points of the B-spline functions, the underlying image is deformed. The B-spline transformation can model local deformations in the image, produces a smooth transformation, and is computationally efficient.[23] The flexibility of the deformation is defined by the resolution of the control point grid.

In the context of the multisequence MR images of the carotid artery, one of the images is chosen as fixed image and the remaining images will each serve as the moving image. Each MR sequence has a different image contrast and the set of sequences can be considered as a multimodal dataset. Therefore, an image similarity metric should be chosen that is suitable for multimodal image pairs, such as MI (Refs. 24 and 25) or Normalized Mutual Information (NMI).[26]

The image similarity metric should only be calculated in a region of interest (ROI) around the carotid artery, otherwise the automatic registration algorithm might align the sequences to the dominant neck-air boundary or other structures. The ROI was implemented by defining an image mask centered over the lumen.

In this study, multiple image registration strategies were investigated to find the optimal strategy for MR vessel wall images of the carotid artery. Strategies were created by varying the choice of the fixed image, two different types of the mutual information image similarity metric, the transformation model and the image mask. The following choices were investigated:

- Fixed image: A human expert often uses one sequence as a reference. In this dataset, the precontrast T1W TSE was chosen to be the reference sequence. However, for automated methods this might not be the best sequence, therefore each of the sequences was tested as fixed image.
- Image similarity metric: MI and NMI were tested as image similarity metrics.
- Transformation model: The selected models were 2D translation per image slice, 2D rigid transform per image slice, 3D rigid transform, 3D affine transform, and 3D B-spline transform. For the 3D B-spline transform, different values of the B-spline control point grid spacing were evaluated. The investigated values ranged from 2 to 200 mm.
- Mask shape and size: The mask was centered over the lumen in the fixed image and various mask shapes and sizes were selected. The shape was either a circle or a square and the respective diameter or width varied from 4 to 40 mm.

2.E. Determination of the lumen center in each image slice

The image mask was centered over the lumen in each image slice of the fixed image. In each slice, the center of the lumen was derived from the gold standard lumen contours. Additionally, the center of the lumen was derived from automated lumen segmentation.[27] This automated procedure was applied to the MR sequence which was evaluated as the best fixed image in Sec. 3.B.2. The segmentation procedure was started by manually indicating a point in the lumen center in the first and the last slice, and subsequently the lumen was segmented. In some cases, a third point was indicated around the bifurcation to ensure a correct segmentation.

2.F. Quantitative evaluation

Evaluation of the automatic registration was performed by comparing the lumen segmentations of the fixed image and moving image after registration. In the case of successful registration, the lumen segmentations should have a large overlap and a small surface to surface distance. The gold standard lumen contours were used for this validation. Both the overlap and distance between the segmentations were used to quantify the registration accuracy.

The automatic image registration finds a coordinate transformation which is defined as a mapping from the fixed image to the moving image. Therefore, the lumen contours of the fixed image are transformed to the moving image domain, in which both contours can be compared to each other. Because the transformed contour can move outside the 2D image plane after a 3D registration, it is not possible to compare the contours on a per slice basis. To be able to compare the results of both 2D and 3D registrations, the lumen contours were converted into 3D tubular surface meshes. The surface mesh was created by interpolating a 3D tubular surface through the contours using linear interpolation.

The overlap between the lumen surfaces was calculated using the Dice similarity coefficient (DSC).[28] The DSC was calculated as follows:

$$\mathrm{DSC} = \frac{2\,|L_{\mathrm{FT}} \cap L_M|}{|L_{\mathrm{FT}}| + |L_M|}, \tag{3}$$

where L_{FT} represents the transformed lumen segmentation of the fixed image, L_M the lumen segmentation of the moving image, and $|\cdot|$ denotes the number of voxels within the segmentation. A DSC of 1 indicates perfect overlap between both lumen surfaces, a value of 0 means that there is no overlap between the surfaces.

The distance between the lumen surfaces was calculated by sampling points on the surface each 0.05 mm. Sampled points on the transformed fixed lumen surface which were positioned outside the moving image domain, points above or below the slice stack of the moving image, were discarded. Then for each point on the transformed fixed lumen surface, the distance to the closest point on the moving lumen surface was calculated. The average of the distances was defined as the mean surface distance (MSD)

$$\mathrm{MSD} = \frac{1}{n}\sum_{i=1}^{n} \min_{q\in L_M} \sqrt{\|\boldsymbol{p_i} - \boldsymbol{q}\|^2}, \tag{4}$$

where $\boldsymbol{p_i}$ is a point on the transformed fixed lumen surface, n is the number of points on the transformed fixed lumen surface, and $\boldsymbol{q}$ is a point on the moving lumen surface. A smaller distance indicates a better registration result. The MSD and DSC scores are summarized by using the median including the interquartile range (IQR) indicated by the plus minus sign and boxplots. The IQR is the difference between the 75th and the 25th percentiles. To compare different registration strategies with either the manual alignment or an automated registration strategy, the Wilcoxon signed rank test was applied to the MSD and DSC scores. A p-value smaller than 0.05 was considered to indicate statistical significance.

3. EXPERIMENTS AND RESULTS

Three experiments were conducted to investigate several aspects of the registration of multispectral MR vessel wall images of the carotid artery. In the first experiment, the need for registration was investigated by analyzing the manual alignments performed by the expert to quantify the amount of patient motion per MR study. In the second experiment, the automatic image registration method was optimized. In the third experiment, we investigated if future improvements of the automated methods are possible. We estimated a lower limit on the registration error by registering the manual lumen segmentations instead of the MR image data.

3.A. Manual alignment

The manual alignments applied by the expert were analyzed to investigate the amount of patient movement within one MR study. For each study, the MR sequences were sorted in chronological order. Then, for each MR sequence, the average applied translation with respect to the first acquired MR sequence was measured per slice and averaged over all slices. As a result, the average translation for the first sequence was zero. This calculation was performed for each study generating 55 averages per MR sequence. The average and standard deviation of these 55 averages were calculated for each MR sequence. For the first ten studies, the time needed to perform the manual alignment was recorded.

The analysis results of the manual alignments are shown in Fig. 2. In total, 1980 image slices were manually aligned (nine slices per sequence, four MR sequences, 55 studies). The average translation per image slice was 1.33 mm. The translations were larger as the patient was longer inside the scanner.

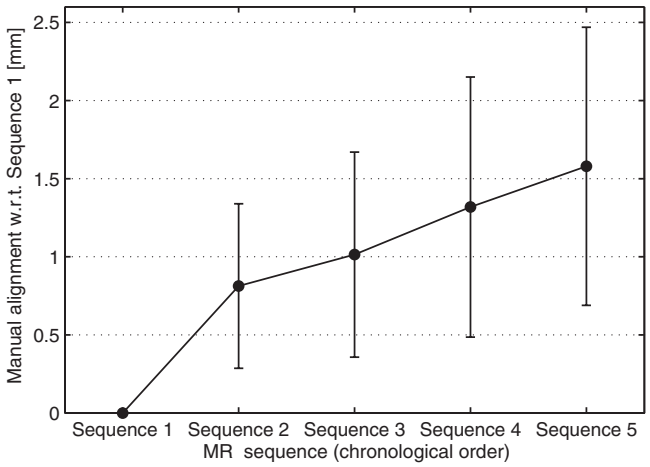

FIG. 2. Average applied manual alignment based on 55 studies and five sequences. The length of the error bars is two standard deviations.

The average duration of the manual alignment procedure was 187.5 ± 12.4 s per patient.

3.B. Automatic image registration

To optimize the automatic image registration method, numerous registration strategies were processed. Different masks, choice of the fixed image, image similarity metrics, and transformation models were evaluated. Investigating all permutations of these options was not feasible due to the required amount of computation time. Therefore, a stepwise approach was taken. First, the effect of the mask shape and size was investigated. A 3D rigid body transformation was chosen, MI as metric, and the precontrast T1W TSE image was used as fixed image. Based on the best mask shape and size, all combinations of fixed and moving images were investigated, again with the same transformation and image metric. Next, the performance of MI and NMI was compared using the optimal fixed image. Then, the optimal value of the B-spline control point grid spacing for the 3D B-spline transformation model was determined. Based on the previously selected registration options, five different transformation models were investigated. For comparison, the MSD of the manual alignments was calculated as well as the MSD in case no registration was applied to the image data. In addition, the DSC was calculated for this experiment. The best registration strategy was evaluated with a mask created using the lumen center extracted from the automated lumen segmentation procedure. Finally, the throughplane translation was quantified for the different 3D registration methods and the amount of volume change was quantified for the 3D B-spline transformation model.

The registration experiments were performed using a speed optimized beta version of the publicly available Elastix software.[21] Elastix is an open source toolbox for rigid and nonrigid registration of images. In this work, a random image sampler, two resolutions of each 1000 iterations, a trilinear image interpolator, and adaptive stochastic gradient descent as optimizer,[29] were chosen. The

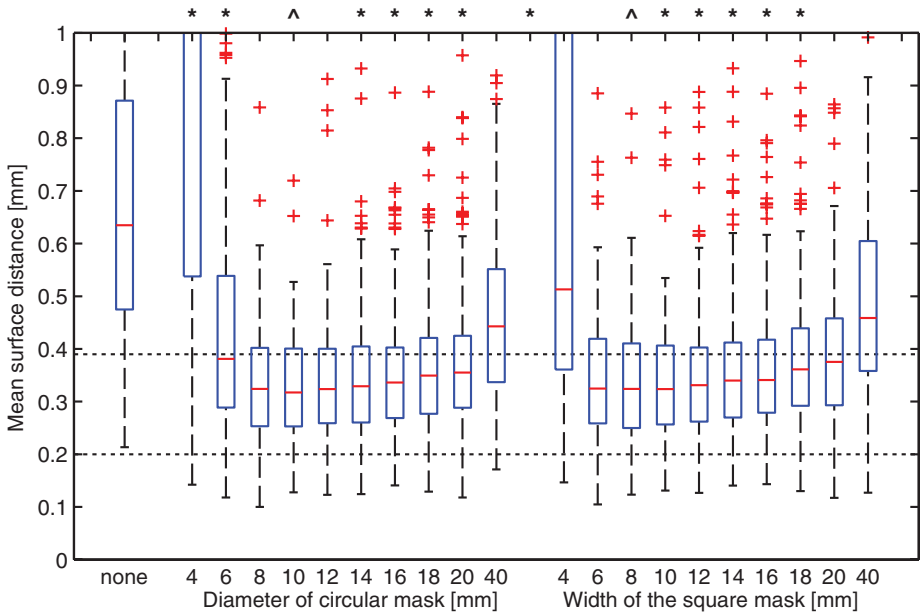

FIG. 3. Mean surface distance for no mask ("none"), circular and square masks of different sizes. A star on top of a column indicates a significant difference with respect to the optimal score of that shape (lowest median), which is indicated by a hat. The two gridlines show the acquired (0.39 mm) and reconstructed inplane pixel size (0.20 mm).

exact registration parameters are available in the parameter file database on the Elastix website with ID Par0018 (http://elastix.bigr.nl/wiki/index.php/Par0018).

3.B.1. Masks

In Fig. 3, a boxplot is shown for the different shapes and sizes of the mask. The optimal circular image mask had a diameter of 10 mm and a MSD of 0.317 ± 0.148 mm. The optimal square mask had a width of 10 mm and a MSD of 0.324 ± 0.150 mm. In case the mask was too small, such that it did not contain the complete vessel, or when no mask was used, large errors appeared. An oversized mask resulted in a larger MSD and an increase in outliers.

3.B.2. Fixed image

Using the optimal mask, all combinations of fixed and moving images were evaluated. The results are shown using a color matrix in Fig. 4. The median MSD and IQR were calculated for each combination of fixed and moving image. The overall score of a fixed image was calculated by accumulating the MSD scores of the four moving image corresponding to the selected fixed image and calculating the median. Using the precontrast T1W TSE as fixed image resulted in the smallest overall MSD while using the TOF as fixed image resulted in the highest MSD. For the further experiments, the precontrast T1W TSE sequence was selected as fixed image.

3.B.3. MI and NMI

Finally, the image similarity metrics MI and NMI were investigated as well as the grid size for the deformable B-spline transformation. MI as image similarity metric performed slightly better than NMI, the MSD was 0.317 ± 0.148 and 0.324 ± 0.156 mm for MI and NMI, respectively.

3.B.4. B-spline control point grid spacing

Different values of the B-spline control point spacing were evaluated using MI as image similarity metric. A control point spacing of 15 mm for the 3D B-spline transformation provided the best results (Fig. 5), and the results were quite stable for grid spacings in the range 5–100 mm.

3.B.5. Transformation model

The MSD for the different transformation models using the optimal mask, fixed image, image metric, and control point spacing is shown in Fig. 6. The first column of the boxplot shows the distance without applying any form of registration (0.590 ± 0.429 mm). The second column shows the results after manual alignment by the expert (0.271 ± 0.127 mm). The remaining columns show the different transformation models: 2D translation per image slice (0.303 ± 0.276 mm), 2D rigid transformation per image slice (0.308 ± 0.298 mm), 3D rigid transformation (0.317 ± 0.148 mm), 3D affine transformation (0.307 ± 0.149 mm), and the 3D B-spline transformation (0.288 ± 0.128 mm). The last column shows the MSD obtained by the best registration strategy using the optimal mask which was initialized by the automatically segmented lumen contours (0.286 ± 0.144 mm). Similarly, the DSC scores are shown in Fig. 7.

The performance of the automated methods increased with an increasing degree of freedom of the transformation model. The 3D B-spline registration showed the best registration accuracy and the MSD score was close to the MSD score of the manual alignment procedure. The differences in

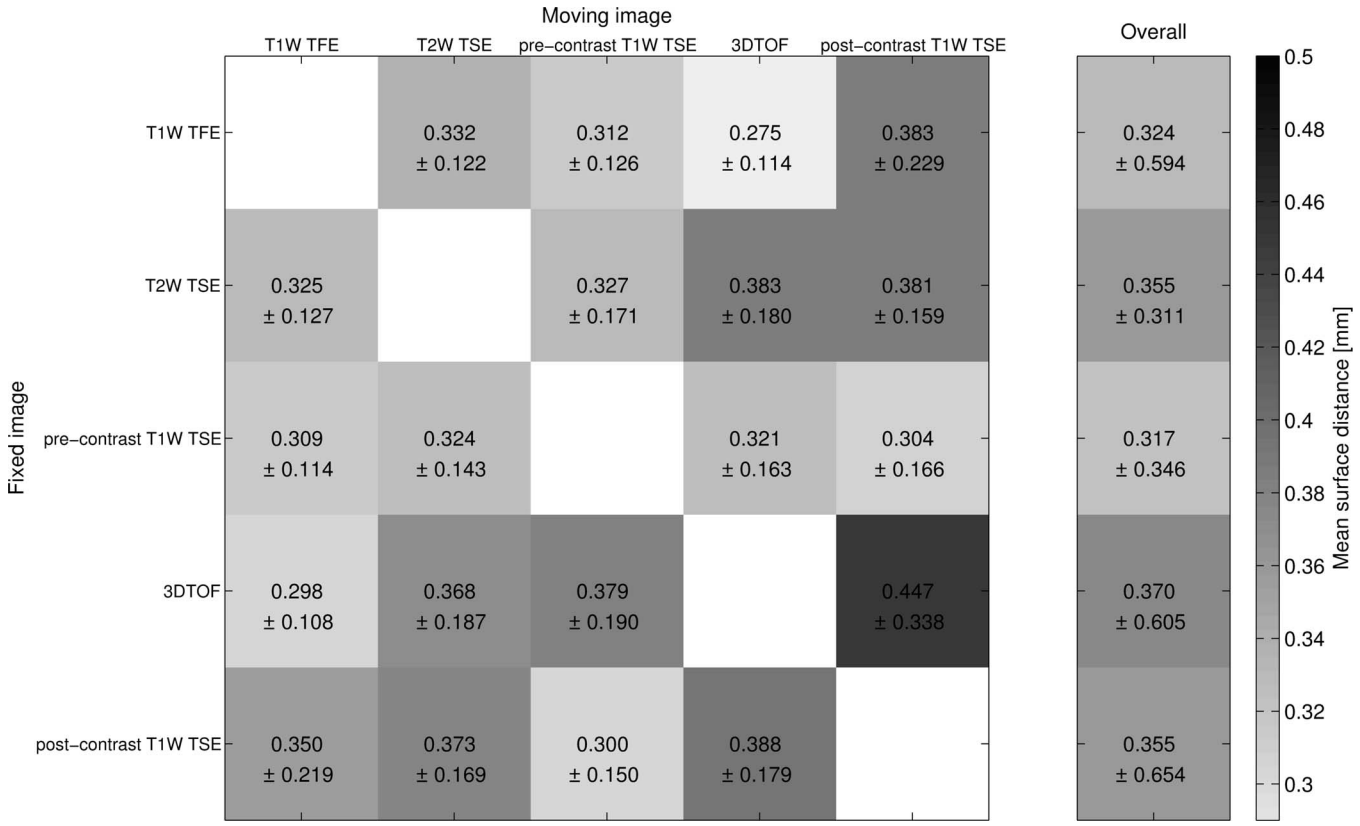

FIG. 4. Color matrix showing the median MSD and the interquartile range of the different combinations of fixed and moving images. The rightmost column shows the overall score for each selected fixed image.

DSC were smaller compared to the differences in MSD. The 2D models showed substantial more outliers and a higher variation in MSD and DSC scores compared to the 3D models. Visual used to investigate the outliers. The majority of outliers were caused by poor image quality in either the fixed or the moving image, pulsation artifacts, or saturation slabs close to the carotid artery. The saturation slabs were positioned over subcutaneous fat to reduce ghosting artifacts and over the pharynx to reduce swallowing artifacts.

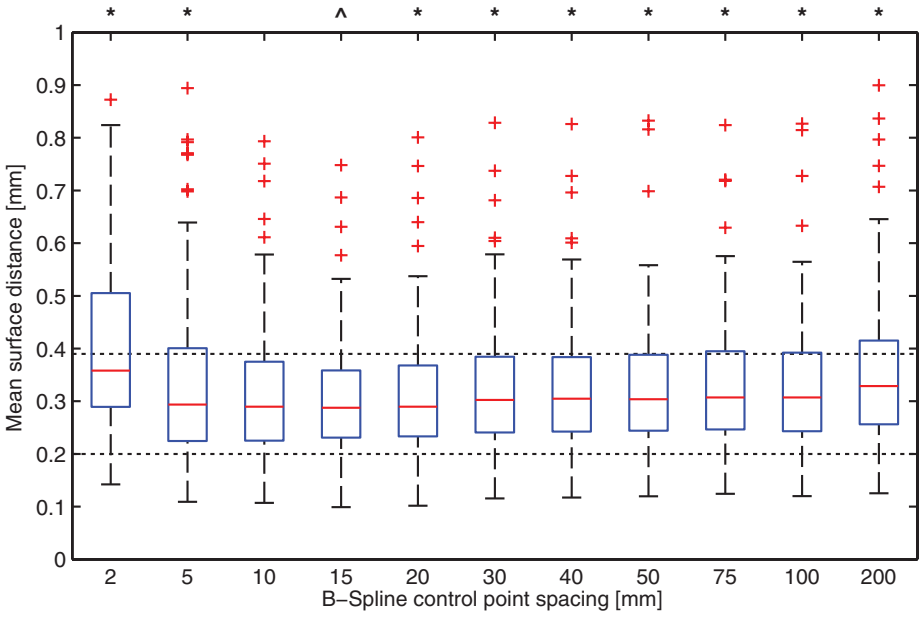

FIG. 5. Mean surface distance for different values of the control point spacing of the 3D B-spline transform. A star on top of a column indicates a significant difference with respect to the optimal spacing, which is indicated by a hat. The two gridlines show the acquired (0.39 mm) and reconstructed inplane pixel size (0.20 mm).

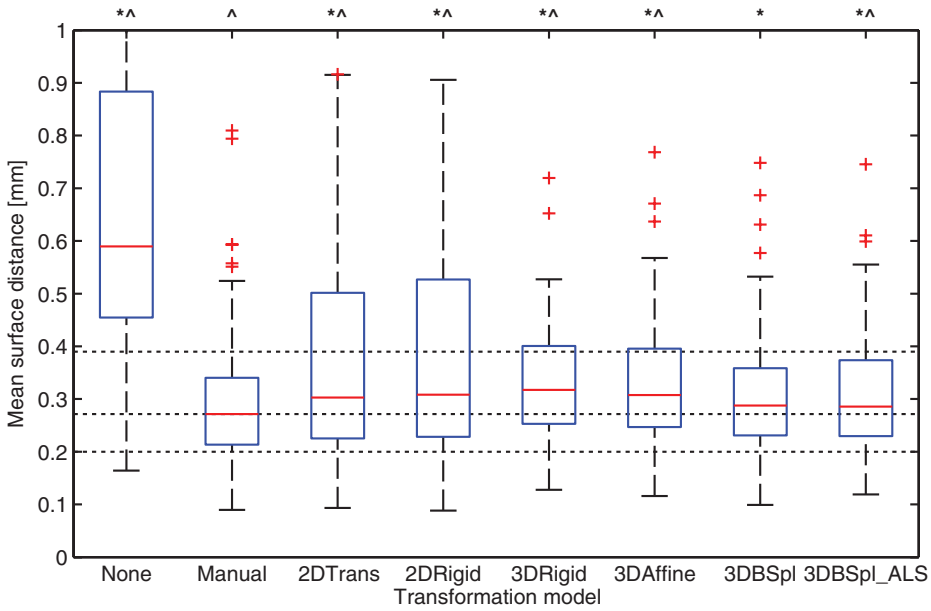

FIG. 6. Mean surface distance for all transformation models (None: no alignment, Manual: manual alignment by the second expert, 2DTrans: 2D translation per image slice, 2DRigid: 2D rigid transform per image slice, 3DRigid: 3D rigid transform, 3DAffine: 3D affine transform, 3DBspl: 3D B-spline transformation, 3DBspl_ALS: 3D B-spline transformation with a mask based on the automated lumen segmentation). A star on top of a column indicates a significant difference with respect to the manual alignment procedure. A hat on top of the figure indicates a significant difference with the 3D B-spline model. The three gridlines show the acquired (0.39 mm) and reconstructed inplane pixel size (0.20 mm) and the median MSD (0.27 mm) of the manual alignment procedure.

The inplane and throughplane translation as a result of a 3D registration was quantified by calculating the average translation of the lumen segmentation in these directions for each 3D registration. The average inplane translation was 1.093 ± 0.913 mm and the average throughplane translation was 0.738 ± 0.571 mm.

The volume change occurring in the deformable 3D B-spline transformation was quantified by calculating the average determinant of the Jacobian of the deformation field within the fixed mask. A value of 1 indicates no volume change, a value of 1.1 indicates local expansion of 10%, and a value of 0.9 indicates local compression by 10%. The mean

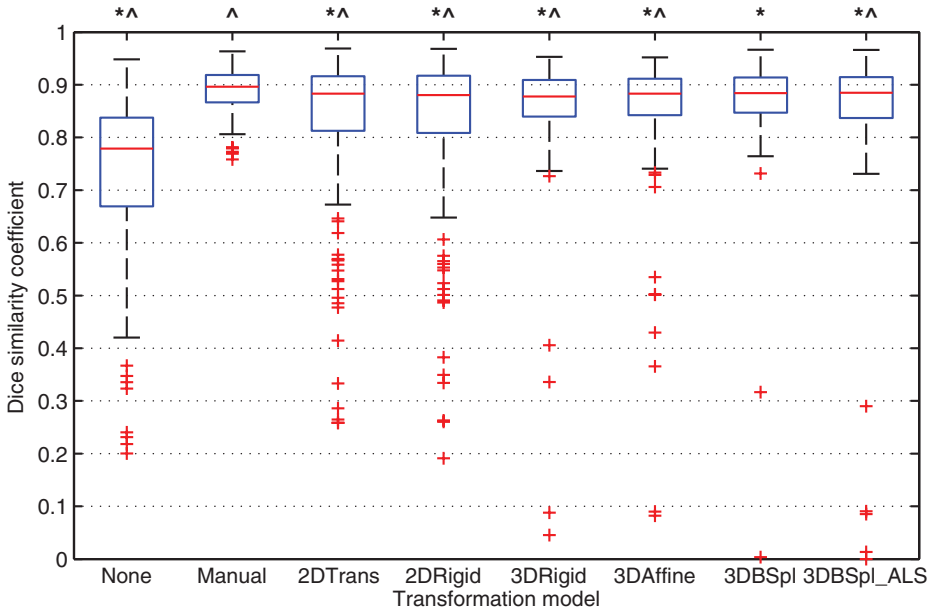

FIG. 7. Dice similarity coefficient for all transformational models (None: no alignment, Manual: manual alignment by the second expert, 2DTrans: 2D translation per image slice, 2DRigid: 2D rigid transform per image slice, 3DRigid: 3D rigid transform, 3DAffine: 3D affine transform, 3DBspl: 3D B-spline transformation, 3DBspl_ALS: 3D B-spline transformation with a mask based on the automated lumen segmentation). A star on top of a column indicates a significant difference with respect to the manual alignment procedure. A hat on top of the figure indicates a significant difference with the 3D B-spline model.

and standard deviation of the Jacobian determinant over all patients was 1.00 ± 0.11, showing no systematic change in volume.

The computation time for the registration of one MR sequence with the precontrast T1W TSE sequence was on average 41.4 s for the 2D translation transform (4.6 s per image slice), 73.8 s for the 2D rigid transformation (8.2 s per image slice), 5.1 s for the 3D rigid transform, 5.0 s for the 3D affine transform, and 13.0 s for the 3D B-spline transform. The registration experiments were performed on a standard PC equipped with an Intel Xeon processor with four cores running at 2.4 GHz. An example of a 3D B-spline registration is shown in Fig. 8. The postcontrast T1W TSE image shows that throughplane correction is required for correct alignment.

3.C. Lower limit registration accuracy

To investigate the lower limit of the registration accuracy, the real image data of each sequence was replaced with a binary mask of the gold standard contours of the lumen of that sequence. Areas within the lumen were set as foreground (intensity value 1), areas outside the lumen as background (intensity value 0). These masks were then used as the fixed and moving images in the registration procedure. Instead of using MI as image similarity metric, the sum of squared differences was used. The automatic image registration was applied on the data to fit the lumen segmentations upon each other. By using the binary lumen masks, perfect image quality is simulated and the results will show an upper bound of the registration accuracy using the current choice of registration parameters.

The lower limit MSD and the regular MSD scores are shown in Fig. 9. The values of the lower limit MSD are smaller for transformation models which have more degrees of freedom, but the medians are in all cases larger than the reconstructed pixel size.

4. DISCUSSION

The main observation of this study is that automated image registration of multicontrast MR imaging of the carotid vessel wall using a 3D B-spline transform is almost as accurate as the current clinical practice of manual alignment by an expert, with final accuracy in the order of the inplane voxel size. The required user-interaction to generate the lumen masks to focus the registration was reduced from one mouse-click per image slice to only two or three mouse-clicks per MRI exam. In addition, automated analysis is at least three times faster than manual alignment of the image data and can potentially be an order of magnitude faster if run in parallel. This paper has a number of contributions. First, the need for alignment of multispectral MR vessel wall images of the carotid artery was quantified. Second, an optimized automatic registration strategy was proposed after investigating and optimizing different parameters of the registration method. Third, a validation framework was proposed which allows comparison of registration results with a gold standard. In addition, an estimate of the maximum performance was derived. This is the first study to quantify these aspects on a large set of patients.

Analysis of the manual alignment by the expert shows the need for registration of carotid MRI studies. The average misalignment per image slice is 1.33 mm, but can be over 2.4 mm, and occurs in all three dimensions. Such a misalignment causes mismatches in pixel correspondence between MR sequences; for example, a location in the vessel wall in one MR sequence can correspond to the lumen area in another MR sequence. If the images are not correctly aligned, manual segmentation of the vessel wall and its components might not be accurate, especially at the boundaries of plaque components. In case an automated plaque segmentation method is applied to the image data, incorrect results are expected, as these methods classify pixels into plaque components according to their signal intensity value in the different MR sequences.[8–10,30]

The different automatic image registration experiments showed in a stepwise fashion the optimal registration

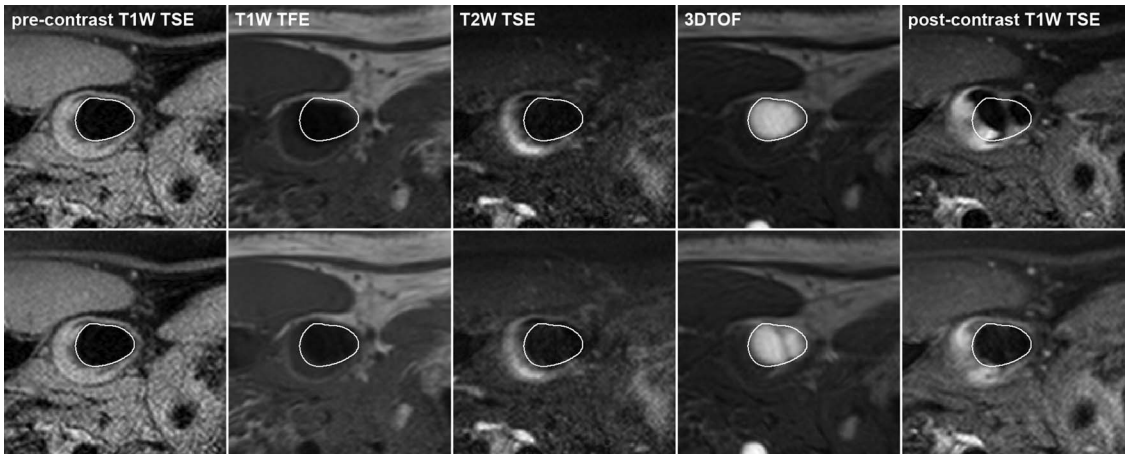

FIG. 8. Example of MRI images before (top row) and after registration by the optimal 3D B-spline transformation (bottom row). The fixed image is shown in the first column. The lumen contour of the fixed image (white) is overlaid on all images. The postcontrast T1W TSE image shows that throughplane correction, which is achieved by using a 3D transformation model, is required for correct alignment.

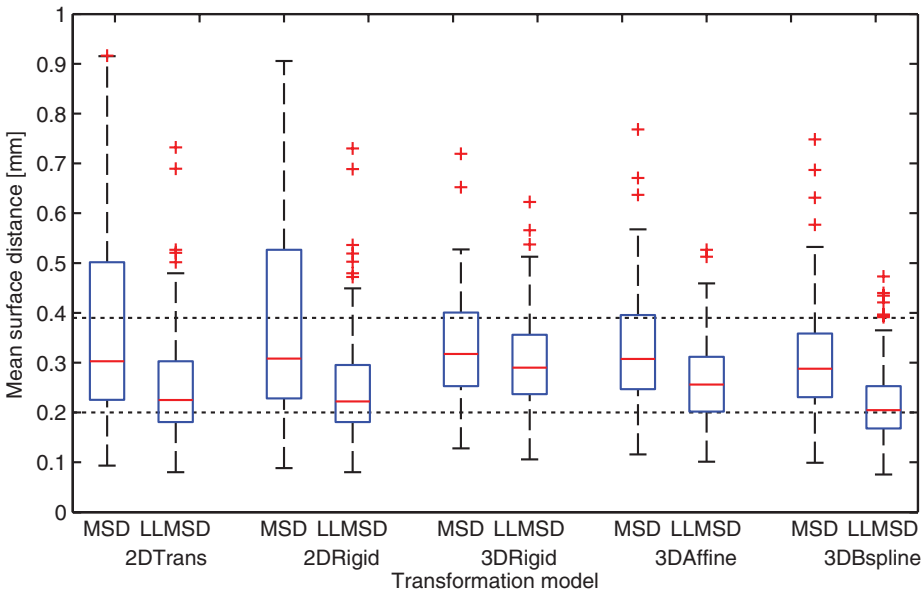

FIG. 9. MSD and lower limit mean surface distance (LLMSD) of the different transformation models (2DTrans: 2D translation per image slice, 2DRigid: 2D rigid transform per image slice, 3DRigid: 3D rigid transform, 3DAffine: 3D affine transform, 3DBspline: 3D B-spline transformation). The two gridlines show the acquired (0.39 mm) and reconstructed inplane pixel size (0.20 mm).

strategy. The building blocks of the registration were optimized to an automated circular mask with a diameter of 10 mm, 3D B-spline transformation model with a control point spacing of 15 mm, MI as image similarity metric, with the precontrast T1W TSE as fixed image. After an indication of the lumen centerline in the T1W image, the other sequences are automatically registered with a median mean surface error of 0.288 ± 0.128 mm. As a reference, the error after manual alignment was 0.271 ± 0.127 mm. The computation time for the registration of the MR sequences was 52.0 s per patient. This is much faster than the time needed for manual alignment, which was 187.5 s per patient. Average run time can potentially be further reduced by a factor of 3–4 by running all registrations in parallel.

The shape and size of the optimal image mask should cover the luminal area, the vessel wall, and its direct surrounding. The experiments have shown that most image information necessary for successful registration is contained in this region and that neighboring structures, such as veins and muscles, do not have an important contribution to the registration process. The optimal mask, a circular mask with a diameter of 10 mm, is slightly larger than the dimensions of the carotid artery including the vessel wall. Krejza *et al.*[31] reported an average internal diameter of the internal carotid artery of 4.89 and 6.31 mm for the common carotid artery. The average vessel wall thickness measured by MRI is 0.92 ± 0.21 mm in elderly subjects with cardiovascular disease.[32]

The selection of the fixed image was investigated and the precontrast T1W-TSE sequence was chosen as fixed image. This is the same image that was used by the human expert as reference. The relatively large MSD for the TOF sequence can be explained by the lack of vessel wall depiction in this sequence. Also the selection of the postcontrast T1W TSE sequence as fixed image showed a relatively large MSD. This sequence is always acquired at the end of the study resulting in a higher chance that the subject will move. Moreover, the administration of contrast agent might cause discomfort for the patient and can result in extra patient motion as a reaction to this discomfort. Furthermore, uptake of the contrast agent results in an increase of heterogeneity in the vessel wall intensities which might decrease the performance of the MI image similarity metric. The matrix of MSD scores in Fig. 4 shows moderate reflection symmetry. Perfect reflection symmetry matrix was not expected as the used registration framework is not symmetrical.

After comparing MI and NMI as image similarity metric and optimizing the control point grid spacing for the 3D B-spline transformation, all transformation models were compared. The best registration accuracy was achieved by using the 3D B-spline transformation model. Although the medians of the MSD and the Dice overlap do not show a substantial improvement for the 3D transformations compared to the 2D transformations, Figs. 6 and 7 show that the 3D transformations have substantially less outliers. Clinically, this means that much fewer patients will need manual correction, saving costly reviewing time by the radiologist. Moreover, analysis of the manual segmentations and the 3D registration results showed that patient movement occurs in all three directions and that throughplane translation is in the same order of magnitude as inplane translation. The nonrigid 3D B-spline transformation model showed an improvement over the rigid 3D transformations. A nonrigid model can better handle rotation of the neck which can cause compression and expansion of tissues. Literature indicated that patient movement includes a nonrigid component.[15,16] Analysis of the deformation fields of the 3D B-spline registrations shows that small local compressions or expansions occur during registration, but on average there was no change in volume. Finally, Fig. 5 shows

that patient motion can be modeled well with a few degrees of freedom.

While the differences in registration accuracy between the different transformation models are small, a nonrigid 3D transformation model is required to correctly model patient movement and obtain an accurate alignment. The 3D B-spline transformation model has the best registration accuracy and the results show that a 3D model is needed because the throughplane motion is in the same range as the inplane motion. An illustrative example of throughplane motion is shown in Fig. 8. The 3D B-spline transformation model performs slightly worse than the manual alignment procedure. Visual inspection of the results showed that most of the differences can be explained by errors of the automated registration of the 3DTOF sequence caused by the lack of structural information in this sequence. By excluding the 3DTOF sequence from the experiment, the MSD of the 3D B-spline transformation model approaches the MSD of the manual alignment and is no longer significantly different. The 3D B-spline registration with the mask based on the automated lumen segmentation performed similarly to the 3D B-spline registration with the mask that was based on the manual segmentation. This shows that the automatic image registration can be applied with minimal user interaction.

The lower limit MSD was found to be slightly larger than the reconstructed inplane pixel size. The comparison shows that the results of the different registration strategies are close to the lowest possible MSD. Hence, major reductions in MSD are not expected by further optimizing or changing the registration strategies, but improvements might still lead to more accurate registration results possibly beating the manual alignment procedure. The minimum value of the lower limit MSD might be limited by the gold standard contours. These contours will vary slightly between the MR sequences because of possible patient movement and human variation in the delineation process. For example, if the lumen contours in one sequence were drawn slightly larger than in another sequence, it will not be possible to obtain a MSD of zero.

Compared to previously reported studies on automatic registration methods for carotid MR vessel wall imaging, this is the first study in which comprehensive experiments were performed on a large set of patient studies using quantitative validation measures. Only one study performed quantitative validation on simulated neck movements in five volunteers.[12] The authors performed the validation in 2D and assumed that neck movements through the image plane and tissue deformations in the image plane were either absent or negligible. However, patient movement occurs in all directions and as such, a 3D image registration approach has advantages, which is supported by our findings. Also, as the thickness of imaging slices will decrease in the future due to technological advancements, the effects of throughplane motion will have a more prominent effect. Two studies[13,14] used a 3D-based registration method being a rigid body transformation or affine transformation. Our results show that such a transformation model is insufficient to generate a good result. Our data suggest that deformations, such as bending and stretching,[33] should be taken into account when choosing a registration strategy.

This study is subject to a number of limitations. An image mask centered over the lumen is required as input for the automatic image segmentation method. This mask can be created by the application of an automated method to segment the carotid lumen,[27,34] which requires a minimal user interaction of two or three interactions per MRI exam as performed in this study.

Motion between slices, which can occur during a 2D acquisition in which the slices are scanned sequentially, was not investigated. We assume that the effect is small compared to the motion between MR sequences. During the acquisition of one sequence, the patient is instructed not to move and most likely will move after completion of the sequence. The error metrics used in this research cannot detect an erroneous rotation in case the vessel is mostly circular. However, the MRI acquisition is centered on the bifurcation and the error metric is sensitive to the rotation of both bifurcations and ellipsoid-shaped vessels. The registration of the multispectral MR vessel wall images is just one of the steps in the analysis of atherosclerosis in the carotid artery. The final step of the analysis is the assessment of plaque composition inside the vessel wall. Accurate alignment of the images is beneficial for the analysis of the plaque composition. More research should be conducted to test if there is a difference in outcome of the plaque composition analysis between manual alignment and automatic image registration.

To conclude, the need for image registration using a 3D deformable transformational model was shown, and several carefully selected, critical components of the registration procedure were optimized and quantitatively validated on a large group of patients. The optimal registration strategy was faster than manual alignment by a human expert, and with similar accuracy. These results show that automated image registration can replace the manual alignment, thus reducing the amount of user interactions needed for analyzing carotid vessel wall images and improving the reproducibility of the analysis. The proposed method shows high potential for clinical application. The software and the parameters of the optimal registration strategy are publicly available.

The main findings of this paper, which were acquired with data from a 1.5T scanner, were validated on a more recent 3.0T dataset. The results of the 3.0T dataset are in line with the results of the 1.5T dataset and show that the same registration settings can be applied to newer MRI data. A short report is available in the supplementary material.[35]

ACKNOWLEDGMENTS

This research was performed within the framework of CTMM, the Center for Translational Molecular Medicine (http://www.ctmm.nl), project PARISk (Grant No. 01C-202), and supported by the Dutch Heart Foundation. The authors thank Dirk H. J. Poot, Ph.D. (Biomedical Imaging Group Rotterdam, Department of Radiology and Department of Medical Informatics, Erasmus MC, Rotterdam, The Netherlands) for providing the optimized nearest neighbor search algorithm

which was used in the calculation of the mean surface distance, and Martine T. B. Truijman (Department of Radiology, Maastricht University Medical Center, Maastricht, The Netherlands) for supplying the 3.0T dataset which was used in the supplementary material.

[a]Author to whom correspondence should be addressed. Electronic mail: rvdgeest@lumc.nl; Telephone: +31 71 526 2138.

[1]V. L. Roger *et al.*, "Heart disease and stroke statistics–2011 update: A report from the American Heart Association," Circulation **123**(4), e18–e209 (2011).
[2]A. J. Lusis, "Atherosclerosis," Nature (London) **407**(6801), 233–241 (2000).
[3]C. Yuan, M. Oikawa, Z. Miller, and T. Hatsukami, "MRI of carotid atherosclerosis," J. Nucl. Cardiol. **15**(2), 266–275 (2008).
[4]C. Yuan *et al.*, "Contrast-enhanced high resolution MRI for atherosclerotic carotid artery tissue characterization," J. Magn. Reson. Imaging **15**(1), 62–67 (2002).
[5]V. C. Cappendijk *et al.*, "Assessment of human atherosclerotic carotid plaque components with multisequence MR imaging: Initial experience," Radiology **234**(2), 487–492 (2005).
[6]C. Yuan *et al.*, "*In vivo* accuracy of multispectral magnetic resonance imaging for identifying lipid-rich necrotic cores and intraplaque hemorrhage in advanced human carotid plaques," Circulation **104**(17), 2051–2056 (2001).
[7]J. F. Toussaint, G. M. LaMuraglia, J. F. Southern, V. Fuster, and H. L. Kantor, "Magnetic resonance images lipid, fibrous, calcified, hemorrhagic, and thrombotic components of human atherosclerosis *in vivo*," Circulation **94**(5), 932–938 (1996).
[8]J. M. A. Hofman *et al.*, "Quantification of atherosclerotic plaque components using *in vivo* MRI and supervised classifiers," Magn. Reson. Med. **55**(4), 790–799 (2006).
[9]R. van 't Klooster *et al.*, "Automated versus manual *in vivo* segmentation of carotid plaque MRI," AJNR Am. J. Neuroradiol. **33**(8), 1621–1627 (2012).
[10]F. Liu *et al.*, "Automated *in vivo* segmentation of carotid plaque MRI with morphology-enhanced probability maps," Magn. Reson. Med. **55**(3), 659–668 (2006).
[11]I. M. Adame, R. J. van der Geest, B. A. Wasserman, M. Mohamed, J. H. C. Reiber, and B. P. F. Lelieveldt, "Automatic plaque characterization and vessel wall segmentation in magnetic resonance images of atherosclerotic carotid arteries," Proc. SPIE **5370**, 265–273 (2004).
[12]L. Biasiolli, J. A. Noble, and M. D. Robson, "Multicontrast MRI registration of carotid arteries in atherosclerotic and normal subjects," Proc. SPIE **7623**, 76232N (2010).
[13]B. Fei, J. S. Suri, and D. L. Wilson, "Three-dimensional volume registration of carotid MR images," Stud. Health Technol. Inform. **113**, 394–411 (2005).
[14]H. Tang *et al.*, "Semiautomatic carotid lumen segmentation for quantification of lumen geometry in multispectral MRI," Med. Image Anal. **16**(6), 1202–1215 (2012).
[15]T. Ohya *et al.*, "Analysis of carotid artery deformation in different head and neck positions for maxillofacial catheter navigation in advanced oral cancer treatment," Biomed. Eng. Online **11**, 65–1–14 (2012).
[16]S. W. Robertson, C. P. Cheng, and M. K. Razavi, "Biomechanical response of stented carotid arteries to swallowing and neck motion," J. Endovasc. Ther. **15**(6), 663–671 (2008).
[17]R. M. Kwee *et al.*, "Symptomatic patients with mild and moderate carotid stenosis: Plaque features at MRI and association with cardiovascular risk factors and statin use," Stroke **41**(7), 1389–1393 (2010).
[18]R. M. Kwee *et al.*, "Multimodality imaging of carotid artery plaques 18F-fluoro-2-deoxyglucose positron emission tomography, computed tomography, and magnetic resonance imaging," Stroke **40**(12), 3718–3724 (2009).
[19]I. M. Adame, R. J. van der Geest, B. A. Wasserman, M. A. Mohamed, J. H. C. Reiber, and B. P. F. Lelieveldt, "Automatic segmentation and plaque characterization in atherosclerotic carotid artery MR images," MAGMA (N.Y.) **16**(5), 227–234 (2004).
[20]W. R. Crum, T. Hartkens, and D. L. G. Hill, "Non-rigid image registration: Theory and practice," Br. J. Radiol. **77**(Spec No. 2), S140–S153 (2004).
[21]S. Klein, M. Staring, K. Murphy, M. A. Viergever, and J. Pluim, "Elastix: A toolbox for intensity-based medical image registration," IEEE Trans. Med. Imaging **29**(1), 196–205 (2010).
[22]S. Klein, M. Staring, and J. P. W. Pluim, "Evaluation of optimization methods for nonrigid medical image registration using mutual information and B-splines," IEEE Trans. Image Process. **16**(12), 2879–2890 (2007).
[23]D. Rueckert, L. I. Sonoda, C. Hayes, D. L. Hill, M. O. Leach, and D. J. Hawkes, "Nonrigid registration using free-form deformations: Application to breast MR images," IEEE Trans. Med. Imaging **18**(8), 712–721 (1999).
[24]P. Viola and W. M. Wells III, "Alignment by maximization of mutual information," Int. J. Comput. Vis. **24**(2), 137–154 (1997).
[25]F. Maes, A. Collignon, D. Vandermeulen, G. Marchal, and P. Suetens, "Multimodality image registration by maximization of mutual information," IEEE Trans. Med. Imaging **16**(2), 187–198 (1997).
[26]C. Studholme, D. L. G. Hill, and D. J. Hawkes, "An overlap invariant entropy measure of 3D medical image alignment," Pattern Recogn. **32**(1), 71–86 (1999).
[27]R. van 't Klooster *et al.*, "Automatic lumen and outer wall segmentation of the carotid artery using deformable three-dimensional models in MR angiography and vessel wall images," J. Magn. Reson. Imaging **35**(1), 156–165 (2012).
[28]L. R. Dice, "Measures of the amount of ecologic association between species," Ecology **26**(3), 297–302 (1945).
[29]S. Klein, J. P. Pluim, M. Staring, and M. A. Viergever, "Adaptive stochastic gradient descent optimisation for image registration," Int. J. Comput. Vis. **81**(3), 227–239 (2009).
[30]S. E. Clarke, R. R. Hammond, J. R. Mitchell, and B. K. Rutt, "Quantitative assessment of carotid plaque composition using multicontrast MRI and registered histology," Magn. Reson. Med. **50**(6), 1199–1208 (2003).
[31]J. Krejza *et al.*, "Carotid artery diameter in men and women and the relation to body and neck size," Stroke **37**(4), 1103–1105 (2006).
[32]R. Duivenvoorden *et al.*, "*In vivo* quantification of carotid artery wall dimensions: 3.0-Tesla MRI versus B-mode ultrasound imaging," Circ. Cardiovasc. Imaging **2**(3), 235–242 (2009).
[33]N. D. Nanayakkara, B. Chiu, A. Samani, J. D. Spence, J. Samarabandu, and A. Fenster, "A 'twisting and bending' model-based nonrigid image registration technique for 3-D ultrasound carotid images," IEEE Trans. Med. Imaging **27**(10), 1378–1388 (2008).
[34]I. M. Adame, P. J. H. de Koning, B. P. F. Lelieveldt, B. A. Wasserman, J. H. C. Reiber, and R. J. van der Geest, "An integrated automated analysis method for quantifying vessel stenosis and plaque burden from carotid MRI images: Combined postprocessing of MRA and vessel wall MR," Stroke **37**(8), 2162–2164 (2006).
[35]See supplementary material at http://dx.doi.org/10.1118/1.4829503 for a report on validation of the found registration settings using a 3.0T MRI dataset.